Chemical Engineering Science 63 (2008) 4418 – 4432

Contents lists available at ScienceDirect

Chemical Engineering Science

journal homepage: www.elsevier.com/locate/ces

On the dynamics and control of through-plane water distributions in PEM fuel cells

Buz A. McCain[a,*], Anna G. Stefanopoulou[a,1], Ilya V. Kolmanovsky[a]

[a]Department of Mechanical Engineering, University of Michigan, 1231 Beal Ave, Ann Arbor, MI 48108, USA

ARTICLE INFO

Article history:
Received 14 January 2008
Received in revised form 12 May 2008
Accepted 14 May 2008
Available online 27 May 2008

Keywords:
Model reduction
Porous media
Dynamic simulation
Diffusion
Control
Stability
Transient response

ABSTRACT

We provide a semi-analytic solution to simplify an experimentally validated numeric realization of a two-phase, reaction–diffusion, distributed parameter model of the through-plane water distributions as they evolve inside polymer electrolyte membrane (PEM) fuel cell gas diffusion layers. The semi-analytic solution is then analyzed for stability and to gain insight into the dynamics of the equilibrium (steady-state) water distributions. Candidate distributions for vapor and liquid water are then identified which allow maximum membrane hydration while simultaneously avoiding voltage degradation that results from anode liquid water accumulation (flooding). The desired anode water distributions could be maintained via control of the anode channel conditions (boundary value control) with the ultimate goal to maximize the hydrogen utilization and prolong fuel cell life.

1. Introduction and motivation

Polymer electrolyte fuel cells (PEFC) are electrochemical energy conversion devices that convert the chemical energy of supplied reactants (hydrogen and oxygen) into electricity. To summarize the operation simply, reactant gases are supplied to both electrodes of the fuel cell via the channels, the gas diffusion layer facilitates even distribution to the catalyst-coated membrane, and the catalyst accelerates the oxidation and reduction of the reactants, which are the primary reactions desired for fuel cell operation (Fig. 1).

The H_2 oxidation on the anode side of the membrane releases two electrons, which then traverse the circuit to satisfy the load required of the cell, while the remaining protons (H^+) travel through the membrane to the cathode side. The O_2 reduction on the cathode side splits the oxygen molecule, which then joins with the electrons completing the circuit and the protons from the membrane to form product water.

The control problem we strive to understand exists because the level of water within the fuel cell directly affects its performance, efficiency, and durability. High-membrane humidity is desirable for proton conductivity, yet excess liquid water has been experimentally shown to be a cause of output voltage degradation (McKay et al., 2008; Siegel and Stefanopoulou, 2008). Specifically, liquid water occupies pore space in the gas diffusion layer (GDL), impedes the diffusion of reactant flow towards the membrane, and ultimately reduces the active fuel cell area, causing performance degradation.

To avoid damage, fuel cells may be operated under flooding conditions (i.e. a net build-up of liquid water). Removal of accumulated liquid water is necessary to regain performance, which is typically accomplished by increasing an inlet flow (anode H_2 or cathode O_2 sources), which results in lower efficiency. Additionally, durability can be compromised by the cycling of the GDL through saturated and sub-saturated conditions that arise from the substantial periodic inlet flow rate changes (purges).

Though cathode flooding is more commonly addressed in the literature (e.g. (Shah et al., 2006; Baschuk and Li, 2000)), we concentrate on anode water management for four reasons. First and foremost, we seek to avoid the anode flooding related voltage degradation demonstrated in the low to medium load fuel cell experiments of McKay et al. (2008) and Siegel and Stefanopoulou (2008) (see e.g. Fig. 5). Second, anode components significantly increase the cost, weight, and size of a fuel cell system. Efficient anode water management will enable the elimination or reduction in equipment for anode inlet humidification and/or recirculation systems (Karnik and Sun, 2005). Third, avoidance of excessive flooding allows higher hydrogen concentrations to be attained, preventing starvation and fuel cell damage due to carbon corrosion. Finally, we desire to implement a flow-through anode channel arrangement to avoid the detrimental effect on GDL material cycling through liquid saturation and drying that occurs during purge cycles in a dead-ended system.

Our goal with this work is to expand and analyze a previously reported semi-analytic solution (SAS) fuel cell water dynamics model

* Corresponding author. Tel.: +1 734 995 2393; fax: +1 734 764 4256.
E-mail address: bmccain@umich.edu (B.A. McCain).

[1] Funding is provided from NSF-GOALI CMS-0625610.

0009-2509/$ - see front matter © 2008 Elsevier Ltd. All rights reserved.
doi:10.1016/j.ces.2008.05.025

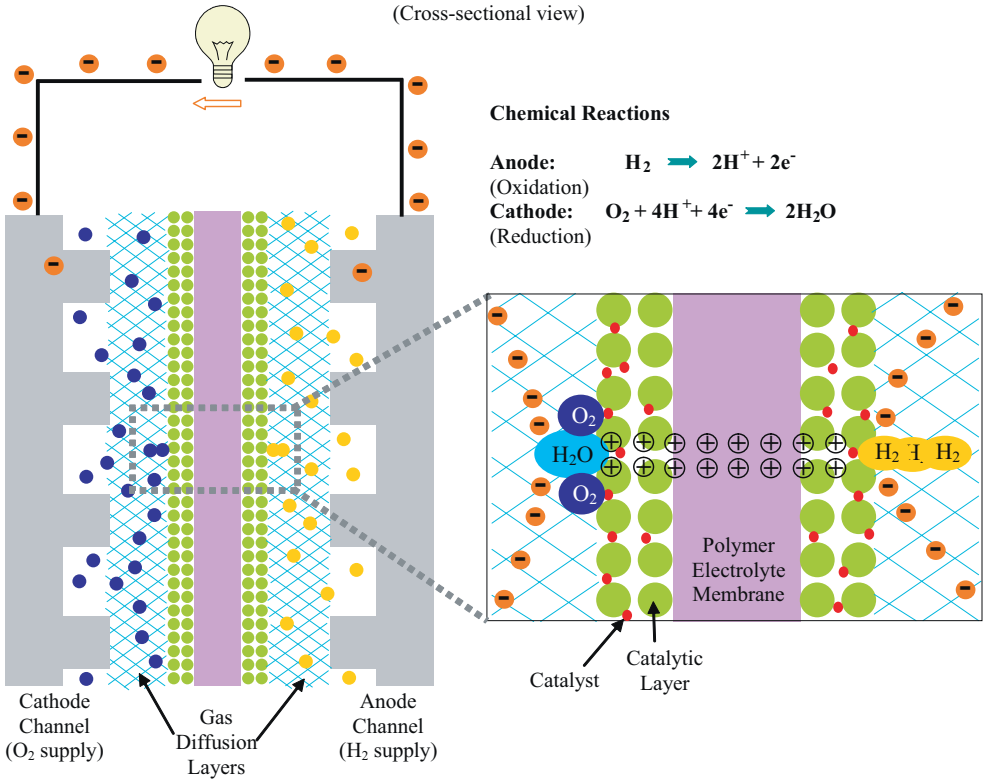

Fig. 1. Schematic representation of fuel cell electrochemistry (not to scale).

(McCain et al., 2007) to demonstrate that it is applicable for water management using automatic control. The SAS model was shown to predict the experimentally observed voltage degradation during operation in a dead-ended anode condition within 1% error versus the full-numeric model of McKay et al. (2008), which was derived from the same partial differential equation (PDE) based model (Section 2). The SAS model reduces the numeric, 24-state, channel-to-channel model to one with just seven-states, four analytic solution equations, and without loss of the physical meanings of the states. The 24-state model has only a three-section spatial discretization of the GDL, providing inadequate understanding of the water distributions, yet pushing the complexity limits for realtime control application. The contribution of the SAS model is reduction in model complexity for the purposes of equilibrium analysis, control application investigation, and greater spatial resolution at equivalent computational cost.

We hypothesize that an appropriate control setpoint is the equilibrium (steady-state) condition where net water flow into the anode GDL is zero and where the water mass transport across the GDL–channel interface is only in vapor phase. This condition is what we term a *borderline* drying condition because it is the point where the boundary between a single-phase and two-phase water distribution lies on the GDL–channel interface *and* there is no liquid flow from GDL to channel. In this work we define the equilibrium points of the model, extend the model of McCain et al. (2007) to include switching water vapor solutions to accommodate the condition where there is a lack of liquid water, which is necessary if the setpoint will be on the cusp of drying, and show that the GDL liquid water volume is a stable system using Lyapunov stability analysis for the liquid water distribution.

Much of the fuel cell modeling upon which this work is based is similar to the work being performed by Promislow (Promislow and Stockie, 2001; Promislow et al., 2008), though we focus on simplification to prepare for a control-oriented application. For example, Promislow includes convective transport, and our assumption of a diffusion-dominated GDL gas transport model allows a simple steady-state analytic solution for the gas constituent distributions to be found, which facilitates stability analysis. Similar to Promislow et al. (2008), we apply quasi steady-state solutions for the gaseous species, recognizing the slow transient nature of the liquid, and we then proceed with emphasis on control analysis. Finally, our water vapor transport is facilitated by a supersaturation-induced concentration gradient, whereas a temperature gradient induces the water vapor transport in Promislow's work.

The recently published work in Grötsch and Mangold (2007) has the similar goal of a two-phase polymer electrolyte membrane fuel cell (PEMFC) model for control by reducing the complexity. The assumptions and focus areas are significantly different; however, with our analysis of the water spatial distributions within the GDLs, inclusion of membrane water vapor transport, and emphasis on avoidance of flooding-induced degradation of voltage output and their simplifying assumptions of lumped values for constituents in the GDL, liquid-only membrane transport, and emphasis on capturing the multiplicities predicted by their high-order model.

Fuel cell control is a growing research interest area, with work expanding in both component and system levels. Modeling and control by Pukrushpan et al. (2000) and Suh and Stefanopoulou (2007) focused on issues associated with control of fuel cells and support components such as compressors run parasitically by the fuel cell. Further, when discussing fuel cell control, the typical meaning is fuel cell power control and the goal is operating the fuel cell efficiently in order to meet the power demands placed on it. Controlled variables for safe and efficient fuel cell operation include oxygen concentration, relative humidity, and power output. In Lauzze and Chmielewski (2006), the control methodology attempted to address all of these varied control objectives by nesting multiple loops. Ideas in the literature for power control include setting a voltage output command to obtain cell current output to meet the power

requirements (or vice versa due to the current–voltage dependency) (Lauzze and Chmielewski, 2006), modulation of oxygen excess ratio via airflow (Mufford and Strasky, 2006), and application of controlled DC/DC converters to convert the fuel cell output to a desired power level (Zenith and Skogestad, 2007). Airflow rate and stack current are the typical control inputs for oxygen starvation prevention (Sun and Kolmanovsky, 2004), while temperature was used as the manipulated variable for humidity control in Lauzze and Chmielewski (2006).

Our focus in this paper is to create a model for prevention of excessive water accumulation in the anode to avoid the associated voltage degradation. At the conclusion of this work, it is expected that the model and control objectives defined will lend themselves to boundary value control, perhaps of the type featured in research on the topic of reaction–diffusion systems of PDEs by Krstic and others (Krstic et al., 2008; Smyshlyaev and Krstic, 2005). By appropriate selection of temperature and H_2 excess ratio (control inputs), we hope to control the channel relative humidity (reference output), which serves as the boundary value of the GDL water vapor distribution. This boundary value shapes the GDL water vapor distribution, which can be used to shape the GDL liquid to a desirable distribution due to the strong influence of the evaporation/condensation reaction on liquid water. These developments will be pursued in separate publications.

The water (liquid and vapor) PDEs are tightly coupled through the evaporation/condensation rate. The liquid water becomes a nonlinearly distributed parameter that inhibits reactant gas and water vapor diffusion. Our model includes channel inlet/outlet conditions and the constituent dynamics within the channel because it is through the channels (lumped with the inlet and outlet manifolds) that the controller can influence the GDL states (liquid water volume, reactant and water vapor concentrations). GDL dynamics are important since the GDL represents the path by which the channel conditions influence the membrane states, and thus the cell performance. The first principles-based constituent dynamics within the GDL used herein, including the capillary flow and porous media gas transport mechanisms, as well as the boundary conditions (BCs), follow closely to that of Nam and Kaviany (2003).

The major contributions of this work include an analysis showing that although unbounded growth of liquid water in the channel (instability) is observed under typical operating conditions, the liquid water distribution within the GDL is exponentially stable. Further, the ranges of possible equilibria for both liquid and vapor water within the GDL are described, leading to the control objective proposal. Simultaneous hydrogen utilization minimization, flooding avoidance, and high-membrane humidification for a flow-through anode will be accomplished by determining the water vapor channel conditions that guarantee zero channel liquid accumulation, preventing unbounded water growth, while maximizing water at the membrane.

2. Model of the GDL

Because creation of a physically intuitive model facilitates controller design and tuning, and since it is currently infeasible to obtain direct, realtime measurements of the critical variables at the membrane and in the GDL, a low-order and compact model of the multicomponent (reactants, water), two-phase (vapor and liquid water), spatially distributed and dynamic behavior across the GDL (Fig. 2) has been investigated. The time-varying constituent distributions in the GDL of each electrode are described by three second-order parabolic PDEs for reactant (oxygen in the cathode and hydrogen in the anode) concentration, water vapor concentration, and liquid water. Instantaneous electrochemical reactions on, and the mass transport through, the catalyst-covered membrane couple the anode and cathode

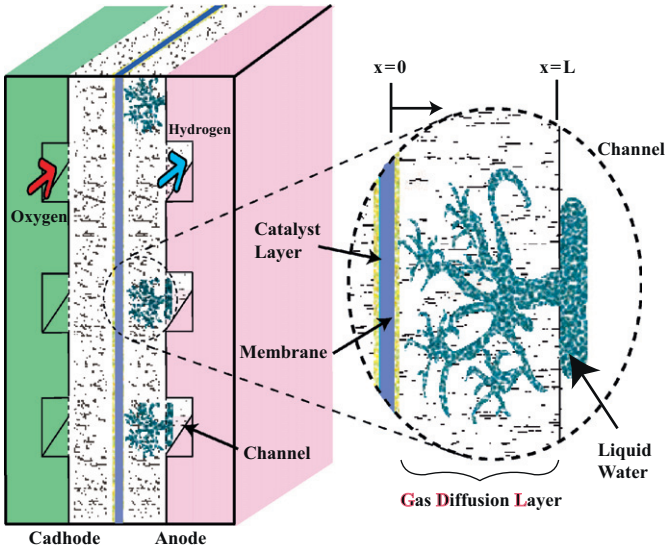

Fig. 2. Accumulation of liquid water in the GDL and subsequent flow to the channel where reactant-blocking film is formed (not to scale).

behaviors and, together with the channel conditions, provide the time-varying boundary values for these PDEs.

2.1. Model assumptions

The non-switching model introduced in McCain et al. (2007) and reviewed herein has the same capability of a completely numeric model to capture the effects of changes to inputs/outputs on voltage estimation. The model combines analytic solutions for the spatial distributions of gases with a numeric solution for the liquid water and was obtained using the following assumptions:

- The model is spatially isothermal, but temperature is allowed to vary in time as this affects inlet and outlet water flow rates as well as the voltage model output. Although the effect of spatial temperature gradients is shown to be important (Djilali and Lu, 2002), the simple tunable isothermal model considered was shown capable of predicting behavior for a reasonable range of conditions.
- Convective (bulk) flow of the gases in the GDL is neglected due to the assumption of very low velocities normal to the membrane.
- Mass transport is in 1D, normal to the membrane, and we neglect the GDL–channel interface variations due to backing plate land and channel interaction. Variation along the channel is also neglected.
- Due to the generation of product water in the cathode GDL, and the fully humidified inlet flow, it is assumed that two-phase water conditions and liquid capillary flow are always present in the cathode. Due to the membrane water transport model employed, cathode liquid water does not influence the anode water distribution, hence we do not model the cathode liquid water. This is done for simplicity only, as the same modeling method used in the anode is applicable to the cathode.
- Water transport out of the anode channel is assumed to be in vapor form due to the low flow rates that will be employed to ultimately achieve high efficiency through high-hydrogen utilization during small flow-through conditions. For a high-velocity channel flow system, this assumption may not be valid (Zhang et al., 2006).
- Though the evaporation model of Mahadevan et al. (2006) includes evaporation even under fully saturated vapor conditions due to the inclusion of compressibility, we employ the simplifying evaporation/condensation model from Nam and Kaviany (2003), where mass flow between the liquid and vapor phases is proportional

to the difference between the water vapor concentration and the concentration at the saturation pressure, i.e. we assume incompressibility.
- There is assumed to be a small, constant, and negligible resistance to liquid flow across the GDL–channel border, represented by a constant S_δ in subsequent equations. Though a modification of this BC would shift the liquid water distribution, it is not expected to significantly alter the qualitative findings of this research.

We proceed with a 1D treatment of the GDL processes, letting x denote the spatial variable, with $x=0$ corresponding to the membrane location and $x=\pm L$ corresponding to the channel locations ($+L$ at anode channel, $-L$ at cathode channel) per Fig. 2, and we let t denote the time variable. The model includes channel and GDL for both anode and cathode, with differences between the electrodes appearing only in sign, rate of reactant consumption, and the generation of water vapor on the cathode side. This water generation is lumped into the membrane transport to form the $x=0$ cathode BC, and thus does not change the form of the equations, only the specific boundary value.

The state variables are as follows:

- $c_{v,\mathrm{an}}(x,t)$ and $c_{v,\mathrm{ca}}(x,t)$ are the concentrations of water vapor at time t at a cross-section of GDL located at x, $0\leqslant x\leqslant L$ (anode) or $-L\leqslant x\leqslant 0$ (cathode).
- $c_{\mathrm{H_2}}(x,t)$ and $c_{\mathrm{O_2}}(x,t)$ are the reactant concentrations at time t at a cross-section of GDL located at x, $0\leqslant x\leqslant L$ (anode-$\mathrm{H_2}$) or $-L\leqslant x\leqslant 0$ (cathode-$\mathrm{O_2}$).
- $s(x,t)$ is the anode GDL fraction of liquid water volume V_L to the total pore volume V_p, $s=V_L/V_p$, commonly referred to as the water saturation. The variable s is thus a concentration-like variable for the liquid water at time t, at a cross-section of GDL located at x, $0\leqslant x\leqslant L$.

The following intermediate variables are useful:

- $N_v(x,t)$ is the water vapor molar flux (mol/m^2/s) at time t at a cross-section of the GDL located at x, $0\leqslant x\leqslant L$ (anode) or $-L\leqslant x\leqslant 0$ (cathode).
- $W_l(x,t)$ is the liquid water mass flow (kg/s) at time t at a cross-section of the GDL located at x, $0\leqslant x\leqslant L$.

2.2. Continuous 1D model formulation

Each of the constituent second-order PDEs are represented by a pair of cascaded first-order PDEs to accommodate the flux/flow-related BCs at the membrane. The water vapor and reactant gas PDEs are autonomous except for an indirect influence exercised via a liquid water dependent effective diffusivity, whereas the liquid water PDE includes a direct coupling water vapor term.

The molar fluxes are driven entirely by the presence of a concentration gradient (i.e. diffusion), since bulk flow (convection) is neglected:

$$N_{j,e}=-D_{j,e}(s)\frac{\partial c_{j,e}}{\partial x}, \tag{1}$$

where the j subscript refers to any of the gas constituents within the fuel cell, and the subscript e indicates that the equation is applicable for both anode (an) and cathode (ca) electrodes. The $D_{j,e}(s)$ are the effective diffusivities for the gases which depend on the liquid fraction, s, since liquid water reduces diffusivity in the GDL by occupying pore space, and are defined by $D_{j,e}(s)=D_{j,\varepsilon}(1-s)^m$. Here $D_{j,\varepsilon}$ is a constant that depends on GDL porosity (ε), and $m=2$ based on Nam and Kaviany (2003).

The reactant gas conservation equations are of the form

$$\frac{\partial c_j}{\partial t}=-\frac{\partial N_j}{\partial x}, \tag{2}$$

where j in Eq. (2) is limited to $\mathrm{O_2}$ or $\mathrm{H_2}$, and the water vapor conservation equations are of the form,

$$\frac{\partial c_{v,e}}{\partial t}=-\frac{\partial N_v}{\partial x}+r_v(c_{v,e}), \tag{3}$$

where r_v is the evaporation rate defined as

$$r_v(c_{v,e})=\begin{cases}\gamma(c_{v,\mathrm{sat}}-c_{v,e}) & \text{for } s>0,\\ \min\{0,\gamma(c_{v,\mathrm{sat}}-c_{v,e})\} & \text{for } s=0,\end{cases}$$

where γ is the volumetric evaporation coefficient and $c_{v,\mathrm{sat}}$ is the vapor concentration associated with the water vapor saturation pressure. Note that evaporation can only occur if there is liquid water ($s>0$) in the GDL, yet condensation can occur even if $s=0$ (if supersaturation exists).

Under the isothermal conditions assumed in this model, once the production or transport of vapor exceeds the ability of the vapor to diffuse through the GDL to the channel, the vapor condenses at the rate determined by γ, hence supersaturated conditions ($c_v(x)>c_{v,\mathrm{sat}}$) are allowed. The mass flow of liquid water is driven by the gradient in capillary pressure (p_c) due to build-up of liquid water in the porous medium,

$$W_l=-\varepsilon A_{fc}\rho_l\frac{KK_{rl}}{\mu_l}\frac{\partial p_c}{\partial x}, \tag{4}$$

where μ_l is the liquid viscosity, ρ_l is the liquid water density, A_{fc} is the fuel cell active area, and K is the material-dependent absolute permeability. The relative liquid permeability is a cubic function of the reduced water saturation $K_{rl}=S^3$ (Nam and Kaviany, 2003), and p_c is a function of a third-order polynomial (Leverett J-function) in $S(x,t)$, where

$$S(x,t)\triangleq\begin{cases}\dfrac{s(x,t)-s_{\mathrm{im}}}{1-s_{\mathrm{im}}} & \text{for } s\geqslant s_{\mathrm{im}},\\ 0 & \text{for } s<s_{\mathrm{im}}\end{cases} \tag{5}$$

and it should be noted that the electrode subscript e is dropped for the liquid-related variables because only anode liquid is modeled.

Under appropriate conditions, liquid accumulates in the GDL until it has surpassed the immobile saturation threshold (s_{im}), at which point capillary flow will carry it to an area of lower capillary pressure (toward the GDL–channel interface). The immobile water saturation s_{im} works as stiction, i.e. there is no liquid flow unless the water saturation exceeds s_{im}. To facilitate the analytic solution, Eq. (4) is rewritten as

$$W_l=-\varepsilon A_{fc}\rho_l\frac{K}{\mu_l}S^3\frac{\partial p_c}{\partial S}\frac{\partial S}{\partial x}, \tag{6}$$

and using an approximation $(K/\mu_l)S^3(\partial p_c/\partial S)\approx b_1S^{b_2}$,

$$W_l=-\varepsilon A_{fc}\rho_l b_1S^{b_2}\frac{\partial S}{\partial x}, \tag{7}$$

where b_1 and b_2 are fitted parameters (confirmation plot shown in Appendix A).

Conservation of liquid mass is employed to determine the rate of liquid accumulation,

$$\frac{\partial s}{\partial t}=-\frac{1}{\varepsilon A_{fc}\rho_l}\frac{\partial W_l}{\partial x}-\frac{M_v}{\rho_l}r_v(c_{v,e}), \tag{8}$$

where M_v is the molar mass of water.

Combining Eq. (1) with Eq. (3) provides the two second-order parabolic PDEs that govern the water vapor concentrations in the cathode and anode,

$$\frac{\partial c_{v,e}}{\partial t} = \frac{\partial}{\partial x}\left(D_{v,e}(s)\frac{\partial c_{v,e}}{\partial x}\right) + r_v(c_{v,e}). \tag{9}$$

It was shown in McCain et al. (2007) that an approximation of the time-varying $D_{v,e}(s)$ with $D_{v,e}(s_{\text{im}})$ yielded negligible error, and since this makes the diffusivity independent of x, it can be represented by D_v^{sim} for both cathode and anode, and the water vapor PDEs become

$$\frac{\partial c_{v,e}}{\partial t} = D_v^{\text{sim}}\frac{\partial^2 c_{v,e}}{\partial x^2} + r_v(c_{v,e}). \tag{10}$$

A similar result is found from Eqs. (7) and (8) for the water saturation PDE,

$$\frac{\partial s}{\partial t} = \frac{\partial}{\partial x}\left(b_1 S^{b_2}\frac{\partial S}{\partial x}\right) - \frac{M_v}{\rho_l} r_v(c_{v,e}). \tag{11}$$

2.3. Boundary conditions

The choice of BCs is important for the solution of the PDE system described in the previous section. For $c_{v,e}(x,t)$, mixed Neumann–Dirichlet type BC are imposed. The channel (ch) BC is,

$$c_{v,e}|_{x=\pm L} = c_{v,e,\text{ch}} = p_{v,e,\text{ch}}/(RT_{\text{st}}), \tag{12}$$

where R is the universal gas constant, T_{st} is the stack temperature, and the total pressure in the anode channel, $p_{\text{an,ch}}$, depends on the exhaust control valve, $u_{\text{out}}(t)$, to be discussed in Section 3. The anode membrane water vapor BC is

$$\left.\frac{\partial c_{v,\text{an}}}{\partial x}\right|_{x=0} = -\frac{N_{\text{mb}}}{D_v^{\text{sim}}}, \tag{13}$$

which represents the assumption that water enters the GDLs in vapor form only due to the presence of microporous layers between the membrane and GDLs (Nam and Kaviany, 2003; Owejan et al., 2007). The membrane water molar flux N_{mb} is governed by electrosmotic drag and back diffusion, which are driven by current density $i(t)$ (A/m^2) and water vapor concentration variation across the membrane, respectively, and depend on stack temperature. The model for N_{mb} used here is taken from McKay et al. (2008), and takes the general form

$$N_{\text{mb}} = \beta_w(\lambda_{\text{ca}} - \lambda_{\text{an}}) - 2.5\frac{\lambda_{\text{mb}}}{22}\frac{i(t)}{F}, \tag{14}$$

with

$$\beta_w = 3.5\times 10^{-6}\alpha_w\frac{\rho_{\text{mb}}}{M_{\text{mb}}t_{\text{mb}}}\frac{\lambda_{\text{mb}}}{14}\,\text{e}^{-2436/T_{\text{st}}}, \tag{15}$$

where α_w is a tuned parameter, λ_{mb} is the membrane water content (Springer et al., 1991), λ_e are the water contents on either side of the membrane, and F represents Faradays constant. The λ_e are polynomial functions of the $c_{v,e,\text{mb}}$, which are the water vapor concentrations on either side of the membrane ($x=0$). The material and physical parameters of the membrane enter through its density (ρ_{mb}), molecular weight (M_{mb}), and thickness (t_{mb}).

At the catalyst layer of the cathode side, product water is generated as a function of $i(t)$, and thus the Neumann BC contains the net of $N_{v,\text{rct}}$ and N_{mb},

$$\left.\frac{\partial c_{v,\text{ca}}}{\partial x}\right|_{x=0} = \frac{N_{v,\text{rct}} - N_{\text{mb}}}{D_v^{\text{sim}}}, \tag{16}$$

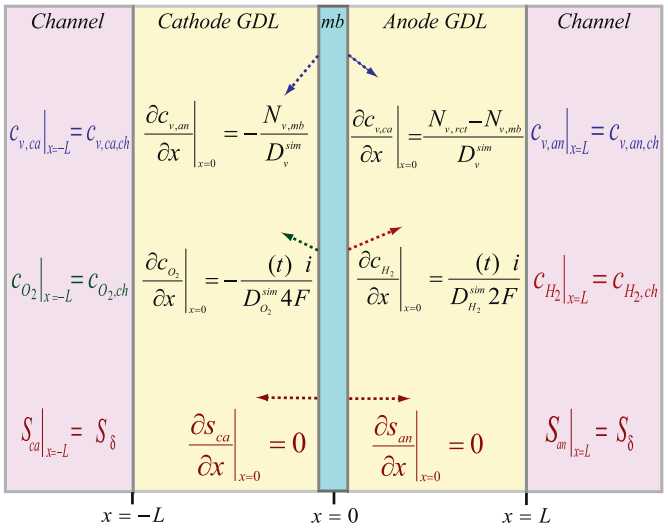

Fig. 3. Boundary conditions for anode and cathode GDL. Time-varying Neumann BC are placed at the membrane, with time-varying Dirchlet BC at the channels (not to scale).

where $N_{v,\text{rct}}$ represents the generation of product water at the cathode catalyst layer given by

$$N_{v,\text{rct}} = \frac{i(t)}{2F}. \tag{17}$$

We will proceed using the assumption that water transport into the GDL at $x = 0$ has no liquid component (Nam and Kaviany, 2003; Owejan et al., 2007). Then for $s(x,t)$, mixed BCs are again imposed:

$$\left.\frac{\partial s}{\partial x}\right|_{x=0} = 0. \tag{18}$$

The setting of a physically meaningful liquid water BC at the GDL–channel interface has been a challenging issue (Shah et al., 2006; Meng and Wang, 2004) with the choice of either zero water saturation or zero liquid flow being typically assumed (Nam and Kaviany, 2003; Siegel et al., 2006; Mazumder and Cole, 2003), though channel water saturation BCs of 0.01, 0.4, and 0.6 were considered in Gan and Chen (2006). A lack of liquid flow into the channel seems physically unlikely and the assumption of zero water saturation ($S|_{x=L} = S_{\text{ch}} = 0$) is convenient for analysis, but does not have a solid physical interpretation. Here we consider the simplifying and convenient form of

$$S(L,t) = S_\delta, \tag{19}$$

where S_δ represents the effect of the liquid water that accumulates on the GDL–channel interface, and the inclusion of S_δ essentially adds a means to provide resistance to flow due to accumulation of liquid in the channel. The value $S_\delta = 0.0003$ was assumed for simulation. For this application the value is independent of the actual amount of liquid in the channel. Based on the voltage output experimental verification, this assumption does not impair the model's estimation ability. However, as more information becomes available from measurement methods such as neutron imaging, this assumption may be reevaluated.

A graphical representation of the BCs described, including appropriately similar BCs imposed on the reactants H_2 and O_2, is shown in Fig. 3.

3. Channel equations

To determine the water vapor channel dynamics, the total channel pressure must be found. The pressures, which represent the channel BCs, are calculated from

$$p_{e,\mathrm{ch}} = \sum_j p_{j,\mathrm{ch}}, \tag{20a}$$

$$p_{j,\mathrm{ch}} = \frac{m_{j,\mathrm{ch}} RT_{\mathrm{st}}}{M_j V_{\mathrm{ch}}} \quad (j \neq v), \tag{20b}$$

$$p_{j,e,\mathrm{ch}} = \min\left\{ \frac{m_{w,e,\mathrm{ch}} RT_{\mathrm{st}}}{M_j V_{\mathrm{ch}}}, p_{v,\mathrm{sat}} \right\} \quad (j = v), \tag{20c}$$

where the subscript j represents each of the gaseous elements present (H_2 and water vapor for the anode, and O_2, N_2, and water vapor for the cathode).

The governing equations for the reactants and water in the channel are

$$\frac{\mathrm{d}m_{j,\mathrm{ch}}}{\mathrm{d}t} = W_{j,\mathrm{in}} + W_{j,\mathrm{GDL}} - W_{j,\mathrm{out}}, \tag{21a}$$

$$\frac{\mathrm{d}m_{w,e,\mathrm{ch}}}{\mathrm{d}t} = W_{v,e,\mathrm{in}} + W_{w,e,\mathrm{GDL}} - W_{v,e,\mathrm{out}}, \tag{21b}$$

where

$$W_{j,\mathrm{in}} = \lambda_j \frac{i(t)}{2\eta F} A_{fc} M_j, \tag{22}$$

with the in and out subscripts referring to channel inlets and outlets, and η is the ratio of atoms per reactant molecule split at the catalyst to the number needed to form one molecule of product water (i.e. η=1 for H_2 and η=2 for O_2), and λ_j is the excess ratio (stoichiometry) of the reactant j.

Differing from the anode inlet, the cathode has a humidified inlet stream, with the relative humidity ($\mathrm{RH}_{\mathrm{ca,in}}$) and the air flow rate ($W_{\mathrm{air,in}}$) prescribed, thus,

$$W_{v,\mathrm{ca,in}} = \frac{\mathrm{RH}_{\mathrm{ca,in}} P_{v,\mathrm{sat,in}}}{P_{\mathrm{air,in}}} \frac{M_v}{M_{\mathrm{air}}} W_{\mathrm{air,in}}. \tag{23}$$

The cathode exit flow rate to the ambient (amb) is another linearly proportional nozzle equation,

$$W_{\mathrm{ca,out}} = k_{\mathrm{ca,out}}(p_{\mathrm{ca,ch}} - p_{\mathrm{amb}}), \tag{24}$$

whereas the anode exit flow rate,

$$W_{\mathrm{an,out}} = u_{\mathrm{out}} \cdot k_{\mathrm{an,out}}(p_{\mathrm{an,ch}} - p_{\mathrm{amb}}) \tag{25}$$

is a controllable valve flow $0 \leqslant u_{\mathrm{out}}(t) \leqslant 1$ to remove both water and hydrogen, and $u_{\mathrm{out}} = 0$ represents a *dead-ended* anode arrangement, which is commonly paired with a periodic purge cycle ($u_{\mathrm{out}} = 1$) for water removal. For $0 < u_{\mathrm{out}} < 1$, this becomes a *flow-through* anode water management system. The model verification of McCain et al. (accepted for publication) was from experimentation that employed the dead-end/purge system, the analysis in this work is applicable for both dead-end and flow-through conditions.

The constituent exit mass flow rates are found from

$$W_{j,\mathrm{out}} = \frac{m_{j,\mathrm{ch}}}{m^{\mathrm{gas}}_{e,\mathrm{ch}}} W_{e,\mathrm{out}}, \tag{26a}$$

$$W_{v,e,\mathrm{out}} = W_{e,\mathrm{out}} - \sum_j W_{j,\mathrm{out}}, \tag{26b}$$

where $m^{\mathrm{gas}}_{\mathrm{an,ch}} = m_{\mathrm{H_2,an,ch}} + p_{v,\mathrm{an,ch}} V_{\mathrm{an}} M_v / (\mathrm{RT}_{\mathrm{st}})$, and j is H_2 for the anode, but addresses both O_2 and N_2 for the cathode.

The hydrogen and water mass flow rate from the GDL to the channel are

$$W_{\mathrm{H_2,GDL}} = -\varepsilon A_{fc} M_{\mathrm{H_2}} \left(D_{\mathrm{H_2}}(s) \frac{\partial c_{\mathrm{H_2}}}{\partial x} \right)\Big|_{x=L}, \tag{27a}$$

$$W_{w,\mathrm{an,GDL}} = -\varepsilon A_{fc} \left(\rho_l b_1 S^{b_2} \frac{\partial S}{\partial x} + M_v D_v(s) \frac{\partial c_{v,\mathrm{an}}}{\partial x} \right)\Big|_{x=L}. \tag{27b}$$

Using the dynamic water mass balance in the channel (21b), the liquid water in the channel is found by assuming that any water in the channel in excess of the maximum that can be held in vapor is liquid,

$$m_{l,\mathrm{an,ch}} = \max[0, m_{w,\mathrm{an,ch}} - c_{v,\mathrm{sat}} M_v V_{\mathrm{ch}}]. \tag{28}$$

This is equivalent to assuming an instantaneous evaporation rate for the channel, and a maximum channel relative humidity of 100%. The channel model structure differs from that of the porous medium GDL, which has an evaporation/condensation rate, and water vapor concentration in excess of saturation is allowed. This differing treatment of the evaporation is simplifying since the channel then does not require separate water vapor and liquid states. For the voltage model of McKay et al. (2008), liquid water mass is of interest, and the approximation of instantaneous evaporation has a very negligible effect on the voltage estimation.

4. The semi-analytic model

In this section an expansion of the semi-analytic model from McCain et al. (2007) is provided, which should be consulted for background details. The time constants of the gas constituents were shown in that work to be much shorter than those of the liquid water, justifying consideration of the quasi steady-state solutions for H_2, O_2, and water vapor when solving for the slowly varying liquid water distributions, assuming liquid water is present throughout the GDL ($s(x,t) > 0$ for $x \in [0, L]$). In this work, we expand the model of McCain et al. (2007) by introducing a moving boundary front between single and two-phase water conditions in the GDL, for which $s(x_{e,\mathrm{fr}}, t) = 0$. The presence of this front necessitates the addition of a set of equations that establish the analytic solution for the conditions where there is only vapor phase water in a range of the GDL. The behavior throughout the GDL can be described with the combined analytic solution that requires switching between the two solutions, hence we have a switching solution system between the range $\{s(x,t) > 0$ for $x \in [0, x_{e,\mathrm{fr}}]\}$ and $\{s(x,t) = 0$ for $x \in [x_{e,\mathrm{fr}}, \pm L]\}$.

4.1. Gas constituent solutions

It is assumed that the front between one and two-phase water will always be two-phase on the membrane side of the front, and if the front is within the GDL, the entire range on the channel side of the front will be single phase. An undesirable example where this would not be true is if the cathode side experienced sudden and significant drying such that the back diffusion not only ceased, but changed direction. That case will not be considered here. It should also be noted that the assumption of consistent cathode liquid water presence implies that the cathode channel water vapor concentration is $c_{v,\mathrm{sat}}(T_{\mathrm{st}})$ for all t.

Following the separation of variables methodology described in McCain et al. (2007), the steady-state solutions for the reactants are

expanded to include the moving boundary at x_{fr}:

$$c_{H_2}(x) = \frac{D_{H_2}^{sim} i(t)}{D_{H_2,\varepsilon} 2F}(x - L) + c_{H_2,ch} \qquad [x_{fr} \leqslant x \leqslant L], \tag{29a}$$

$$c_{H_2}(x) = \frac{i(t)}{D_{H_2}^{sim} 2F}(x - x_{fr}) + c_{H_2}(x_{fr}) \qquad [0 \leqslant x < x_{fr}], \tag{29b}$$

$$c_{O_2}(x) = -\frac{i(t)}{D_{O_2}^{sim} 4F}(x - L) + c_{O_2,ch} \qquad [-L \leqslant x \leqslant 0], \tag{29c}$$

where $c_{H_2}(x_{fr})$ is determined from Eq. (29a), then applied in Eq. (29b).

The steady-state water vapor distributions when $s(x,t) > 0$ are given by

$$c_{v,an}(x) = \alpha_1 e^{\beta x} + \alpha_2 e^{-\beta x} + c_{v,sat} \qquad [0 \leqslant x < x_{fr}], \tag{30a}$$

$$c_{v,ca}(x) = \nu_1 e^{\beta x} + \nu_2 e^{-\beta x} + c_{v,sat} \qquad [-L \leqslant x \leqslant 0], \tag{30b}$$

where

$$\beta = \sqrt{\gamma / D_v^{sim}}. \tag{31}$$

The α_i are functions of N_{mb} and the anode channel condition (i.e. the anode GDL BC),

$$\begin{aligned} &\alpha_1 e^{\beta x_{fr}} + \alpha_2 e^{-\beta x_{fr}} = c_v(x_{fr}) - c_{v,sat}, \\ &\alpha_1 - \alpha_2 = -N_{mb}/\beta D_v^{sim}. \end{aligned} \tag{32}$$

The ν_i, similar to the α_i, are dependent upon N_{mb} and the cathode channel condition, but are additionally influenced by the water vapor reaction term $N_{v,rct}$ from the reformation of H_2O at the cathode catalyst,

$$\begin{aligned} &\nu_1 e^{-\beta L} + \nu_2 e^{\beta L} = c_{v,ca,ch} - c_{v,sat} \\ &\nu_1 - \nu_2 = (N_{v,rct} - N_{mb})/\beta D_v^{sim}. \end{aligned} \tag{33}$$

The membrane water transport, N_{mb}, can be found from Eq. (14), and requires knowledge of the water vapor concentrations on both sides of the membrane, obtained from Eq. (30a) at $x = 0$,

$$\begin{aligned} &c_{v,an,mb} = (\alpha_1 + \alpha_2) + c_{v,sat}, \\ &c_{v,ca,mb} = (\nu_1 + \nu_2) + c_{v,sat}. \end{aligned} \tag{34}$$

The cathode side water vapor concentration is modeled to determine the $c_{v,ca,mb}$, which is necessary to find N_{mb}. However, the focus of our model is anode side water management (though the process developed is equally applicable to the cathode), thus for notation simplification the subscript an will be understood and omitted in subsequent formulation and discussion.

To this point, we have discussed the water vapor model valid for two-phase flow (i.e. $s(x,t) > 0$). We need to consider the water vapor distribution solution for values of x such that $s = 0$ for $x > x_{fr}$ (single-phase GDL conditions). Consideration of this condition requires a switching solution system (discussed in Section 4.3), and the time and spatially varying location of x_{fr}, which is found numerically from the solution of $s(x,t)$ as expressed in Section 4.2.

Within the single-phase water flow condition, the effective diffusivity is constant, so we consider Eq. (10) when the evaporation reaction term has gone to zero,

$$\frac{\partial c_v}{\partial t} = \frac{\partial}{\partial x}\left(D_{v,\varepsilon}\frac{\partial c_v}{\partial x}\right) = D_{v,\varepsilon}\frac{\partial^2 c_v}{\partial x^2}. \tag{35}$$

where $D_{v,\varepsilon} = D_v(0)$ is the vapor diffusivity when $s = 0$.

The steady-state solution of

$$0 = D_{v,\varepsilon}\frac{\partial^2 c_v}{\partial x^2} \tag{36}$$

is

$$c_v^{lin}(x) = m_o(x - L) + c_{v,ch} \text{ for } (x \geqslant x_{fr}), \tag{37}$$

where the slope of the linear distribution, m_o, will be derived in Section 4.3.

4.2. Liquid water solution

It has been shown that the time constants (McCain et al., 2007) of the water vapor modes are more than an order of magnitude faster than those of the liquid water, and that the time constant of the water vapor is proportional to the evaporation rate γ. Using a singular perturbation argument, we replace the c_v coupling term in Eq. (11) by its steady-state solution (30a). The PDE for liquid water distribution in the porous medium is then

$$\frac{\partial s}{\partial t} = \frac{\partial}{\partial x}\left(b_1 S^{b_2}\frac{\partial s}{\partial x}\right) + \frac{M_v \gamma}{\rho_l}(\alpha_1 e^{\beta x} + \alpha_2 e^{-\beta x}), \tag{38}$$

for (x,t) such that $s(x,t) \geqslant s_{im}$, and

$$\frac{\partial s}{\partial t} = \frac{M_v \gamma}{\rho_l}(\alpha_1 e^{\beta x} + \alpha_2 e^{-\beta x}), \tag{39}$$

for (x,t) such that $0 < s(x,t) < s_{im}$ where $S = 0$ per Eq. (5), and β and α_i are as defined in the $c_v(x)$ solution previously (30a).

For the $s(x,t) \geqslant s_{im}$ case, Eq. (38) can be integrated twice to obtain the steady-state liquid water saturation,

$$s^{ss}(x) = \beta_z \left[\beta(\alpha_1 - \alpha_2)(x - L) + c_{v,ch} - c_{v,sat} - (\alpha_1 e^{\beta x} + \alpha_2 e^{-\beta x}) + \left(\frac{S_\delta}{\beta_z}\right)^{b_2+1} \right]^{1/(b_2+1)} + s_{im}, \tag{40}$$

with

$$\beta_z = (1 - s_{im})\left(\frac{M_v \gamma (b_2 + 1)}{\rho_l \beta^2 b_1}\right)^{1/(b_2+1)}. \tag{41}$$

For the $0 < s(x,t) < s_{im}$ case, because it is required for equilibria analysis, the unsteady solution of Eq. (39) can be found easily by integrating with respect to time,

$$s(x,t) = \frac{M_v}{\rho_l}\gamma(\alpha_1 e^{\beta x} + \alpha_2 e^{-\beta x})t + s_0(x), \tag{42}$$

where $s_0(x)$ is the water saturation distribution at $t = t_0$. The $s_0(x)$ term represents the influence of the initial conditions on the water saturation.

Since the complete analytic solution of Eq. (38) has not been found, we therefore proceed by defining a SAS that combines the quasi steady-state analytic solutions for the gas constituents $(c_{H_2}(x), c_{O_2}(x), c_v(x), c_{v,ca}(x))$ with the anode liquid water ratio $(s(x,t))$ numeric differential algebraic equation (DAE).

4.3. Vapor solution transition

In this section we analyze the transition between the two-phase exponential solution (30a) and the linear single-phase solution (37). We assume that total water flux is preserved at the transition from two-phase to single-phase and use mass flow continuity across the

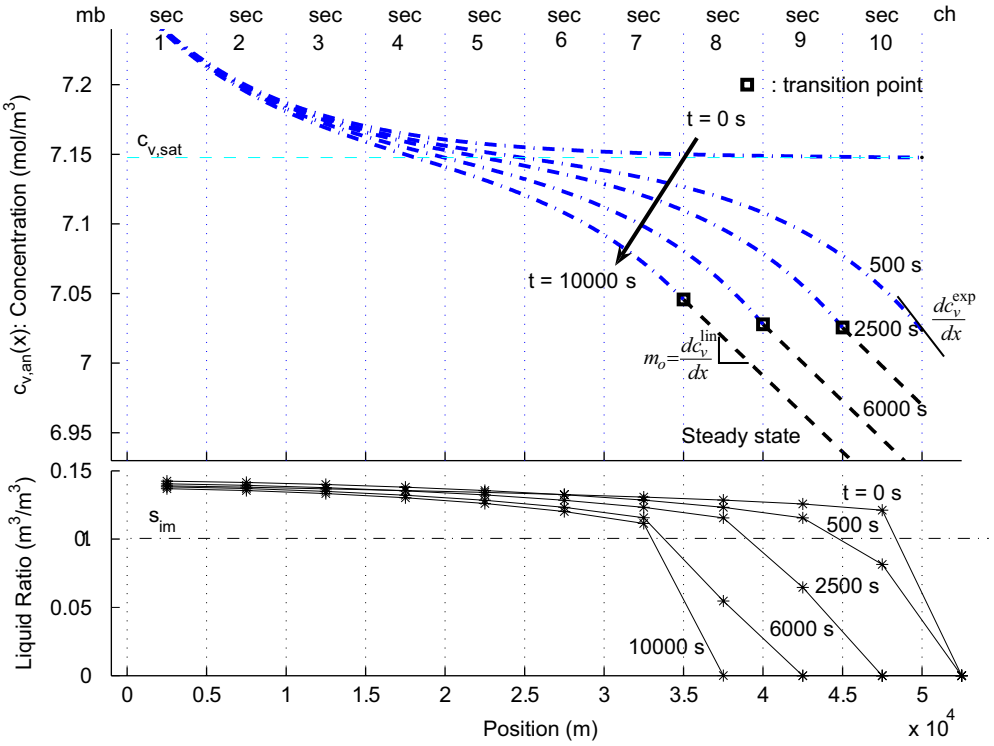

Fig. 4. Water vapor and liquid water distributions for the switching analytic solution. Due to the numeric nature of the liquid solution, each section liquid fill is represented by one point. The connecting lines are only to separate the time snapshots and do not represent the actual distribution.

transition point to establish the necessary flow rate on the single-phase side of the mobile front.

To satisfy mass flow continuity, $W_w^{\text{lin}} = W_w^{\text{exp}}$, which can be shown by manipulation of the definitions of mass flow rates to result in the slope for the single-phase water concentration of Eq. (37),

$$m_o = \frac{D_v^{\text{sim}}}{D_{v,\varepsilon}} \beta(\alpha_1 \, e^{\beta x_{\text{fr}}} - \alpha_2 \, e^{-\beta x_{\text{fr}}}) - \frac{W_l(x_{\text{fr}}^-, t)}{M_v \varepsilon A_{fc} D_{v,\varepsilon}}. \tag{43}$$

Here x_{fr}^- indicates the spatial coordinate of the mobile front that is part of the two-phase water solution, where x_{fr} is defined as the smallest value of x such that $s(x_{\text{fr}}, t) = 0$ from the numeric solution of Eq. (38). The vapor-only water mass flow rate on the single-phase side of x_{fr} must match the sum of the liquid and vapor water mass flow rates on the two-phase side, hence the $W_l(x_{\text{fr}}^-, t)$ term in Eq. (43), which is found by solving Eq. (7) with $S(x_{\text{fr}}^-, t)$. Finally, the α_i are found from Eqs. (32) and (34).

4.4. Simulation of vapor solution transition

A simulation example of the reaction–diffusion to diffusion-only switching solution for a 10-section GDL discretization is shown in Fig. 4. The graph shows the time progression of the water vapor concentration distribution as the liquid water mobile front recedes into the GDL, where Section 1 is the lumped parameter volume closest to the membrane, and Section 10 is closest to the channel. The system is modeled as an averaged single cell of the 24-cell, 300 cm^2 active area, 1.2 kW experimental fuel cell stack set up used in the model verification. The current density is 0.15 A/cm^2, the cathode inlet stream is fully humidified air, the anode inlet stream is pure, dry hydrogen supplied at 2.63 times stoichiometry, and the stack temperature is set at 333 K.

In this example, an initially flooded anode at $t = 0$ s experiences a change to a drying condition due to a 9% increase in H_2 excess ratio. By $t = 500$ s, the channel liquid water has been removed as evidenced by the drop in vapor concentration at $x = L$, but since there is still liquid water in Section 10, the exponential solution is temporarily valid throughout the GDL ($0 \leqslant x \leqslant L$). However, $s(10) < s_{\text{im}}$ indicates that liquid flow into the channel has ceased, implying that GDL–channel water transport is in vapor phase only, with the mass flow rate given by

$$W_w^{\text{exp}}(x_{\text{fr}}^-, t) = -M_v \varepsilon A_{fc} D_v^{\text{sim}} \left. \frac{\partial c_v^{\text{exp}}(x)}{\partial x} \right|_{x = x_{\text{fr}}^-} + W_l(x_{\text{fr}}^-, t) \tag{44}$$

and $W_l(L, t) = 0$. We can conclude that this GDL to channel water flow rate is smaller than the vapor flow rate out of the channel because the two-phase front recedes toward the membrane during the time period 500 s < t < 10 000 s, finding equilibrium when the front reaches Section 7. Thus, Fig. 4 depicts the modeled water vapor distribution of the combined diffusion–reaction/diffusion-only SAS, with the $c_v(x)$ in $x < x_{\text{fr}}$ taking the exponential solution, and the $c_v(x)$ in $x \geqslant x_{\text{fr}}$ taking the linear solution.

5. Observation on system instability

We know from experiment and simulation that the fuel cell in total will experience unbounded liquid water growth under many normal operating conditions (flow regulated anode inlet, high-H_2 utilization, etc). Additionally, modal analysis of the system indicates the presence of unstable modes when linearized about operating conditions with liquid accumulation in the channels.

Fig. 5 demonstrates the basic voltage degradation phenomena seen in our experimentation, and which our model captures; namely that anode flooding is related to voltage degradation. The periodic

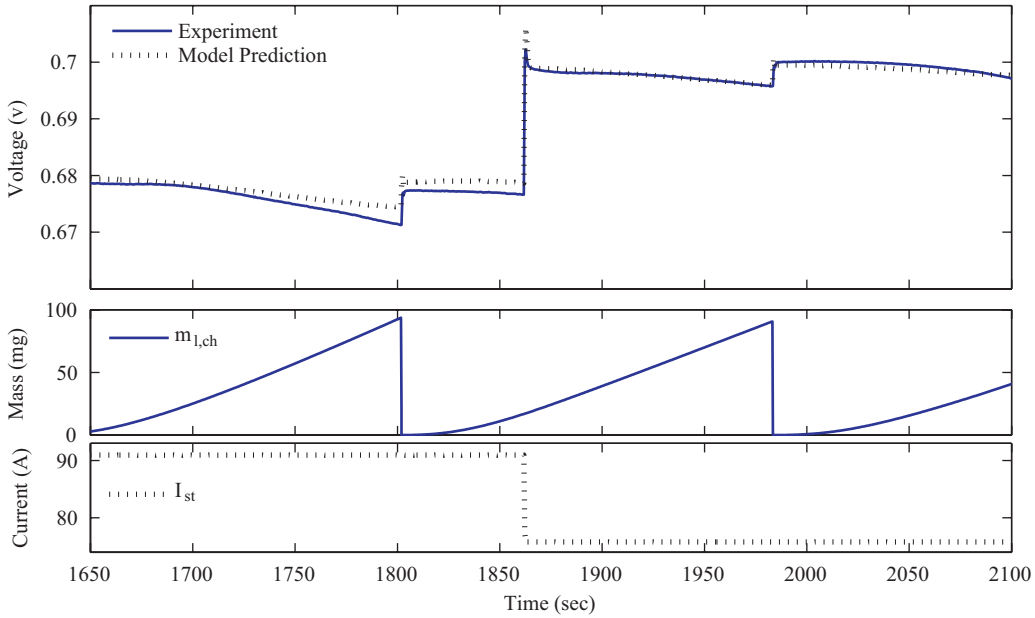

Fig. 5. Experimental results support the hypothesis that anode flooding causes voltage degradation that is recovered through anode channel purging.

purges necessary to remove the anode liquid water, and the recovery of the cell voltage, can be immediately seen. A step-down change in stack current (91 A → 76 A) occurring at a time of low-channel water mass ($t \sim 1862$ s) does not noticeably affect the liquid accumulation, though a voltage output overshoot matching that of the experiment is well estimated.

It turns out that the apparent instability is due to the channel water mass state. Specifically, one can show the following result:

Theorem. *Given the assumptions of Section* 2.1, *the PDEs and BCs described in Sections* 2 *and* 3, *and the SAS from Section* 4, *the liquid water distribution for the anode is stable if the channel liquid water is stabilized.*

Proof (Sketch). The GDL liquid water is exponentially stable (see Appendix A for proof). Therefore, stabilization of the channel water mass state results in overall water system stability. We proceed with analysis to determine a control requirement to stabilize channel water mass. □

6. Analysis of equilibria

Understanding of the system equilibria is a critical step towards definition of control objectives. The form of Eq. (42) suggests that an equilibrium condition for $0 < s(x,t) < s_{\text{im}}$ does not exist because the α_i are not functions of s. This observation raises the need for discussion regarding s_{im}, and an analytic study of the dynamic properties of the model equilibria.

The immobile saturation s_{im} represents the amount of liquid water required to wet the porous material fibers such that continuous liquid flow can proceed. A value of $s_{\text{im}} = 0.1$, or 10% of the pore volume being filled with liquid, is a common value used (Nam and Kaviany, 2003). Others choose to ignore the s_{im} concept, which is equivalent to setting it to zero (Vynnycky, 2007). We proceed following the logic that there will be no liquid flow if the liquid volume is extremely low, and thus the s_{im} value of 0.1 will serve for analysis purposes. It is interesting to note that the choice of s_{im} will affect the liquid water distribution estimation (Gan and Chen, 2006). It is also shown here that the concept of immobile saturation introduces a range of s where equilibrium does not exist.

Analysis of the combined liquid and water vapor SAS and the steady-state liquid water solution (40) reveals that any distribution of c_v that satisfies the steady-state solution (30a) can be an equilibrium water vapor distribution. In this analysis, however, we are most interested in finding c_v equilibria that reduce or prevent build-up of liquid water in the channel.

6.1. Claim: no equilibrium exists for $0 < s(x) < s_{\text{im}}$

We claim that there exists no equilibrium condition such that an $s(x)$ within the GDL is non-zero, but less than the immobile saturation. To see this, we expand the spatial derivative of the first term of Eq. (11) around some x,

$$\frac{\partial s(x,t)}{\partial t} = b_1 \left[b_2 S^{b_2-1}(x,t) \left(\frac{\partial S(x,t)}{\partial x} \right)^2 + S^{b_2}(x,t) \frac{\partial^2 S(x,t)}{\partial x^2} \right] - \frac{M_v \gamma}{\rho_l} (c_{v,\text{sat}} - c_v(x)). \tag{45}$$

When $s(x,t) < s_{\text{im}}$ and since $b_2 > 1$, the two terms within the bracket are zero because $S(x,t) = 0$ ($s(x,t) < s_{\text{im}}$), therefore

$$\frac{\partial s(x,t)}{\partial t} = -\frac{M_v \gamma}{\rho_l} (c_{v,\text{sat}} - c_v(x)). \tag{46}$$

First, considering the cases where $c_v^{ss}(x) \neq c_{v,\text{sat}}$, the RHS of Eq. (46) dynamic equation is not a function of $s(x,t)$, and therefore no condition exists that will satisfy $\partial s/\partial t = 0$. Thus, while $0 < s(x,t) < s_{\text{im}}$, $s(x,t)$ will either grow (positive $\partial s/\partial t$, i.e. $c_v(x) > c_{v,\text{sat}}$) until it exceeds s_{im}, causing S to be re-introduced as an opposing factor for the condensation or decrease under evaporation (negative $\partial s/\partial t$, i.e. $c_v(x) < c_{v,\text{sat}}$), which will cease only when $s(x,t) = 0$.

It remains to show that $c_v^{ss}(x) \neq c_{v,\text{sat}}$ when $0 < s(x) < s_{\text{im}}$.

6.2. Claim: $c_v^{ss}(x) \neq c_{v,\text{sat}}$ for $0 < s(x) < s_{\text{im}}$

We claim that anywhere in the GDL that the liquid saturation steady-state is less than the immobile saturation, the water vapor

pressure will not match the saturation pressure. To demonstrate this, we provide a continuity of solution sketch of argument followed by a physical-insight-based explanation.

The sketch of proof method begins by assuming, in contradiction, that there exists an $\bar{x}$ that satisfies $c_v^{ss}(\bar{x}) = c_{v,\mathrm{sat}}$ and $0 < s(\bar{x}) < s_{\mathrm{im}}$. We claim that when $s(\bar{x})$ falls between zero and s_{im}, it does so on a continuous open interval U around $\bar{x}$, where we know $s(x,t)$ is continuous because the derivative of Eq. (42) exists within $0 < s(x,t) < s_{\mathrm{im}}$.

Continuity in $s(x,t)$ over U implies that an equilibrium value of $s(\bar{x})$ will be accompanied by continuous equilibrium values for all $s(x,t)$ within U. However, it follows from Eq. (30a) that

$$c_v^{ss}(x) - c_{v,\mathrm{sat}} = \alpha_1 \mathrm{e}^{\beta x} + \alpha_2 \mathrm{e}^{-\beta x} = 0 \rightarrow \mathrm{e}^{2\beta x} = -\frac{\alpha_1}{\alpha_2} \tag{47}$$

within U. Since α_1 and α_2 will have constant values in equilibrium, this incorrectly implies that the exponential function $\mathrm{e}^{2\beta x}$ equals a constant over U. Therefore, the original premise is incorrect and there exists no $\bar{x}$ such that a steady-state condition $c_v(\bar{x}) = c_{v,\mathrm{sat}}$ exists when $0 < s(x,t) < s_{\mathrm{im}}$.

The above conclusion can be physically explained by recognizing that the claim is essentially a statement about the location of x_{fr} relative to x_{sat}, defined by $c_v(x_{\mathrm{sat}}) = c_{v,\mathrm{sat}}$.

We know from steady-state mass flow continuity that

$$W_l^{ss}(x) + W_v^{ss}(x) = W_{\mathrm{mb}}. \tag{48}$$

Since both flows are positive in the direction from membrane to channel, the maximum equilibrium liquid flow naturally occurs when $W_v^{ss}(x)$ is at a minimum. Since the molar water vapor flux is directly proportional to the first spatial derivative of $c_v(x)$, this minimum is located at x_{sat}, which can be shown by taking the second derivative of Eq. (30a) with respect to x and setting it to zero,

$$\frac{\partial^2 c_v(x)}{\partial x^2} = \beta^2(\alpha_1 \mathrm{e}^{\beta x} + \alpha_1 \mathrm{e}^{-\beta x}) = \beta^2(c_v(x) - c_{v,\mathrm{sat}}) = 0. \tag{49}$$

Since Eq. (49) is satisfied by $c_v(x) = c_{v,\mathrm{sat}}$, we know that the minimum water vapor transport occurs at $x = x_{\mathrm{sat}}$, thus the steady-state liquid flow rate is a maximum at $x = x_{\mathrm{sat}}$, implying $s(x_{\mathrm{sat}}, t) > s_{\mathrm{im}}$ and therefore $c_v(x) \neq c_{v,\mathrm{sat}}$ for $0 < s(x,t) < s_{\mathrm{im}}$.

Note 1: The steady-state liquid and vapor water transport at any x across the GDL can be calculated as follows:

Beginning with the definition of liquid water mass flow (6) and reversing the chain rule to get the $\partial/\partial x$ to include the S^{b_2} term,

$$W_l = -\varepsilon A_{fc} \rho_l b_1 S^{b_2} \frac{\partial S}{\partial x} = -\varepsilon A_{fc} \rho_l \frac{b_1}{b_2 + 1} \frac{\partial}{\partial x}(S^{b_2+1}). \tag{50}$$

Substituting the steady-state $S^{ss}(x)$ found from Eqs. (5) and (40),

$$\begin{aligned} W_l^{ss} = & -\varepsilon A_{fc} \rho_l \frac{b_1}{b_2+1} \frac{\partial}{\partial x} \left(\frac{M_v \gamma (b_2+1)}{\rho_l \beta^2 b_1} \right. \\ & \times \left[\beta(\alpha_1 - \alpha_2)(x - L) + c_{v,\mathrm{ch}} - c_{v,\mathrm{sat}} \right. \\ & \left. \left. -(\alpha_1 \mathrm{e}^{\beta x} + \alpha_2 \mathrm{e}^{-\beta x}) + \left(\frac{S_\delta}{\beta_z} \right)^{b_2+1} \right] \right) \end{aligned} \tag{51}$$

moving the constants out of the differentiation, rearranging, substituting for β^2 from Eq. (31), differentiating with respect to x we find,

$$W_l^{ss}(x) = -M_v \varepsilon A_{fc} \left[\underbrace{D_v^{\mathrm{sim}} \beta(\alpha_1 - \alpha_2)}_{-N_{\mathrm{mb}}} - \underbrace{D_v^{\mathrm{sim}} \beta(\alpha_1 \mathrm{e}^{\beta x} - \alpha_2 \mathrm{e}^{-\beta x})}_{-N_v(x)} \right], \tag{52}$$

which is a restatement of Eq. (48), since $W_v(x) = M_v \varepsilon A_{fc} N_v(x)$.

Note 2: Eq. (48) clearly indicates that the steady-state liquid flow will match the membrane water transport less than the water vapor transport if there is sufficient liquid present in the GDL to generate capillary flow. Conversely, if capillary flow conditions are not met ($s(x,t) \leqslant s_{\mathrm{im}}$), the entire water transport will be in vapor form. It is important to note that for a given set of system conditions, W_{mb} is constrained by $W_{l,\mathrm{GDL}}$ because as long as $s > s_{\mathrm{im}}$, membrane water transport will not change. Although it might sound counter-intuitive, zero liquid flow across the GDL–channel interface allows greater membrane transport from cathode to anode. Thus the anode conditions can be used to control cathode flooding.

7. Stabilizing equilibrium

Considering the water management goal of minimizing flooding and maximizing membrane hydration, we search for an equilibrium condition with zero liquid flow into the channel and the highest possible water content in the GDL. Of course, this assumes that there exists a stable liquid water distribution in the GDL that does not significantly hinder reactant access to the catalyst. We show GDL liquid stability in Appendix A, and Siegel and Stefanopoulou (2008) used neutron imaging to show that typical steady-state levels of liquid water in the anode GDL do not significantly reduce voltage output, perhaps due to a randomly distributed nature of the liquid within the porous medium.

The top plot of Fig. 6 shows the results from a set of conditions that begin under a state of flooding ($W_{\mathrm{mb}} > W_{v,\mathrm{out}}$), generated with a stack current of 45 A, stack temperature at 333 K, and a hydrogen excess ratio of 2.5. All sections of the 10-section discretization have saturation levels above s_{im}, which will generate an undesirable liquid water flow into the channel and cause the increase in $m_{l,ch}$ seen prior to $t = 1000$ s. At $t = 1000$ s, the H_2 excess ratio (λ_{H_2}) is increased to 2.63, sufficient to dry the anode channel, and force the two-phase water front to recede into the GDL. The transient response of the liquid water (Fig. 6) shows the water saturation of the section closest to the channel (Section 10) being driven to zero, at which time the liquid water in Section 9 begins to fall. The process continues until the front reaches Section 7, attaining equilibrium because GDL flow-in (i.e. W_{mb}) increased to match channel flow-out (i.e. $W_{v,\mathrm{out}}$).

To illustrate the mechanisms leading to equilibrium, consider the lower subplot of Fig. 6 where plots of relevant mass flow rates are shown. The $W_{l,\mathrm{GDL}}$ is sufficient to balance the GDL water mass in the first 1000 s, prior to the λ_{H_2} increase. After $t = 1000$ s, we see from Eq. (52) and Fig. 6 that the liquid water flow decreases in proportion to the increase in water vapor flow resulting from the reduction in channel water vapor concentration caused by the channel water mass imbalance. In physical terms, at the start of a flooding-to-drying transition (i.e. $W_{\mathrm{mb}} > W_{v,\mathrm{out}} \rightarrow W_{v,\mathrm{out}} > W_{\mathrm{mb}}$), the net GDL–channel water flow is insufficient to satisfy the water mass balance in the channel, causing liquid evaporation, net water transport out of the GDL, and a decrease in the channel water vapor concentration below saturation level. The GDL nearest the channel will experience liquid volume decrease as more vapor is drawn by the sub-saturated channel, leading to a decrease in liquid flow to the channel. Once the liquid flow has ceased, the vapor mass flow-out of the GDL continues to increase and can reach flow rates greater than the steady liquid mass flow rate experienced when $m_{l,\mathrm{ch}} > 0$ and $c_{v,\mathrm{ch}} = c_{v,\mathrm{sat}}$. The $W_{v,\mathrm{GDL}}$ is increased by further decreases in $c_{v,\mathrm{ch}}$ until the GDL water equilibrates.

Under transient drying conditions ($W_{v,\mathrm{out}} > W_{\mathrm{mb}}$) the limitation that $W_{l,\mathrm{GDL}}^{ss} < W_{\mathrm{mb}}$ requires channel mass balance be obtained through vapor transport. To establish equilibrium, W_{mb} must increase, and this will happen only when the water vapor GDL–channel transport increases. Until liquid flow reaches zero, any increase in $W_{v,\mathrm{GDL}}$ occurs with a corresponding loss in liquid flow. The $W_{v,\mathrm{GDL}}$

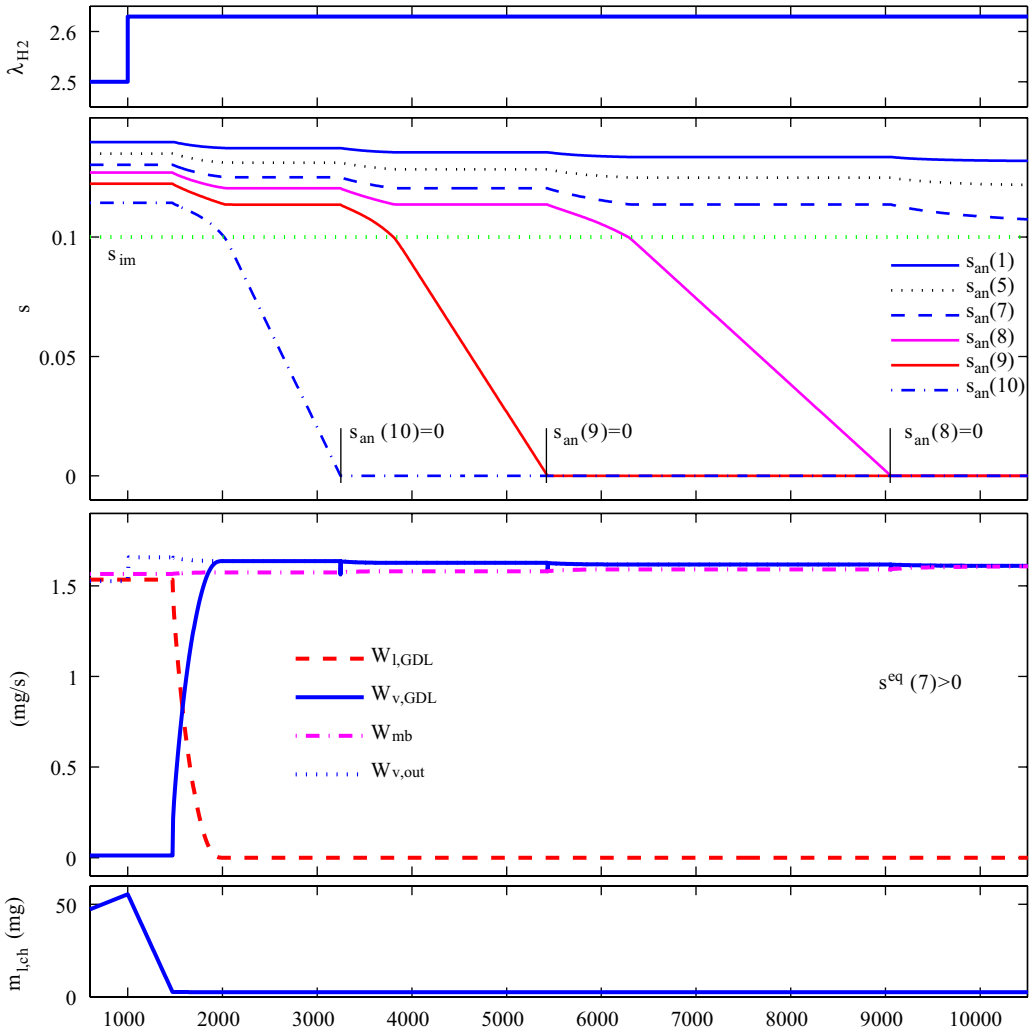

Fig. 6. Initially in a flooding condition, the H_2 excess ratio creates a drying condition. The mobile two-phase water front recedes into the GDL as Section 10, nearest the channel, reaches zero liquid volume. Equilibrium is reached at Section 7 (i.e. $s_{an}(7)>0$). Lower plot: After the liquid water is removed, the water vapor flow increases and W_{mb} increases to match the $W_{v,out}$, which is decreasing due to lowered $c_{v,ch}$.

growth to match $W_{v,out}$ will eliminate $W_{l,GDL}$ as the two-phase front recedes from the channel.

7.1. Claim: $c_{v,ch} = 2c_{v,sat} - c^{ss}_{v,mb}$ implies stable equilibrium and maximum GDL hydration

We claim that a channel water vapor concentration that is below the saturation water vapor concentration by the same amount that $c_{v,mb}$ above it will result in zero liquid flow into the channel and that this will maximize water in the GDL under zero liquid channel flow conditions.

Using the steady-state water vapor solution, the claim implies,

$$(\alpha_1 e^{\beta x} + \alpha_2 e^{-\beta x})|_{x=0} = -(\alpha_1 e^{\beta x} + \alpha_2 e^{-\beta x})|_{x=L} \tag{53}$$

or

$$\alpha_1 + \alpha_2 = -(\alpha_1 e^{\beta L} + \alpha_2 e^{-\beta L}). \tag{54}$$

Maximum GDL hydration will occur when the two-phase front is located at $x = L$, the GDL–channel interface. To find the water vapor concentration at the two-phase front ($c_v(x_{fr}) = c_{v,ch}$) with zero liquid flow into the channel, we use the knowledge that $W_{l,GDL} \to 0$ as $W_{v,GDL} \to W_{v,out}$, and steady-state mass continuity, to show that after $W_{l,GDL} = 0$, $W_{v,GDL} \to W_{mb}$ at equilibrium. Since the mass flow is related to the slope of the water vapor distribution by

$$W_{v,GDL} = -M_v \varepsilon A_{fc} D_v^{sim} \left.\frac{dc_v}{dx}\right|_{x=L} \tag{55}$$

and

$$W_{mb} = -M_v \varepsilon A_{fc} D_v^{sim} \left.\frac{dc_v}{dx}\right|_{x=0}, \tag{56}$$

this implies,

$$\left.\frac{dc_v(x)}{dx}\right|_{x=L} = \left.\frac{dc_v(x)}{dx}\right|_{x=0}. \tag{57}$$

Taking the spatial derivative of Eq. (30a),

$$\frac{dc_v(x)}{dx} = \beta(\alpha_1 e^{\beta x} - \alpha_2 e^{-\beta x}), \tag{58}$$

we see the equality of the water vapor slopes at the boundaries implies,

$$\alpha_1 e^{\beta L} - \alpha_2 e^{-\beta L} = \alpha_1 - \alpha_2, \tag{59}$$

when $N_{mb} = N_{v,GDL}$.

Therefore, to demonstrate the claim, we need only show Eq. (54), which can be done by direct algebraic manipulation after substituting Eq. (59) into both sides of Eq. (54), indicating that, indeed, $c_{v,\mathrm{ch}} = 2c_{v,\mathrm{sat}} - c_{v,\mathrm{mb}}$ when $N_{\mathrm{mb}} = N_{v,\mathrm{GDL}}$. Since $N_{v,\mathrm{GDL}} = N_{\mathrm{mb}}$ implies $W_{l,\mathrm{GDL}} = 0$, system stability may be demonstrated.

8. Control concept

We utilize the fuel cell model's estimation of liquid flow into the channel both for prediction of voltage degradation and as an indication of flooding in the fuel cell that is highly detrimental to fuel cell performance and longevity. The semi-analytic model of the liquid water and water vapor distributions can be utilized to control anode channel liquid water accumulation, and thus potentially avoid voltage output degradation due to excessive water in the cell. The issue of the appropriate channel liquid water BC (19) can be avoided completely by setting the control objective for the channel water vapor concentration such that the liquid water BC at $S(L,t) = 0$, thus stabilizing the nominally unstable channel liquid water dynamics.

Fig. 7 demonstrates that the steady-state solution to the water vapor PDE has an exponential form, while the liquid PDE is a fractional power polynomial. These shapes are highly dependent upon the choice of BC, as evidenced by results from Natarajan and Nguyen (2001), where numeric results show much higher liquid ratios ($s > 0.80$) at the membrane and zero liquid water at the channel, due to the assumptions of liquid water transport across the membrane and $s = 0$ at the GDL–channel interface. Recent results (Owejan et al., 2007) support the membrane BC (18) used here.

The dash–dot line in Fig. 7 demonstrates that liquid water in excess of the immobile saturation (i.e. flooding) exists in the GDL when the water vapor concentration has reached its maximum value of $c_{v,\mathrm{sat}}$ in the channel. Under these conditions, the liquid water will grow unbounded in the channel (instability). The solid line represents a lower channel water vapor concentration, and we observe a channel condition ($c_{v,\mathrm{ch}} = c^*_{v,\mathrm{ch}}$) below which the GDL two-phase boundary begins to recede into the GDL (stable with $x_{\mathrm{fr}} = L$). The dotted line depicts the steady-state distributions if $c_{v,\mathrm{ch}} < c^*_{v,\mathrm{ch}}$, where the two-phase water front has receded into the GDL (stable with $s(L^-) = 0$).

The water vapor concentration at the vapor transition, $c_v(x_{\mathrm{fr}})$, plays a key role in our model. Regardless of the position, it represents the BC for the exponential solution. Based on the Section 7.1 *Claim*, we propose that

$$c^*_{v,\mathrm{ch}} = 2c_{v,\mathrm{sat}} - c^{ss}_{v,\mathrm{mb}} \tag{60}$$

is a control objective that satisfies equilibrium, eliminates GDL–channel liquid transport, provides channel stability, and maintains the membrane water content at the highest value for a given set of conditions. A discussion on the practicality of the defined control objective follows in *Note* 3.

Note 3: The volumetric evaporation constant (γ), taken for this work from Nam and Kaviany (2003), plays a significant role in determining the $c^*_{v,\mathrm{ch}}$. For $\gamma = 900\,\mathrm{s}^{-1}$, it is likely that $c^*_{v,\mathrm{ch}}$ will be within 2% of saturation, and use of the outlet humidity near saturation as the reference output presents an issue of sensor resolution and function. Near saturation, typical sensors can become clogged with liquid, rendering them temporarily ineffective. These issues may be resolved with heated, high-resolution sensors, or with innovative control algorithms. Further, the $c^*_{v,\mathrm{ch}}$ reference value is an upper

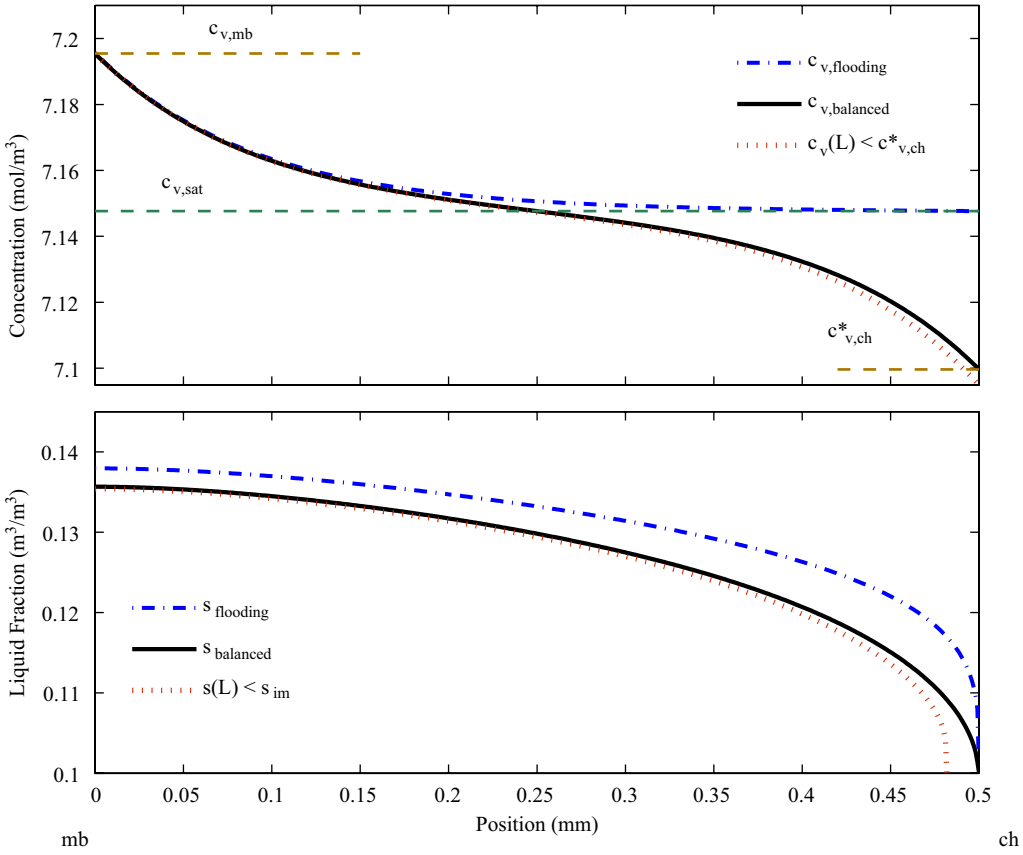

Fig. 7. Anode distribution of liquid water ratio for varying channel water vapor concentrations illustrates that the channel water vapor concentration boundary value can shape the liquid water distribution. The flooding case has $c_{v,\mathrm{ch}} = c_{v,\mathrm{sat}}$, while the borderline case has $c_{v,\mathrm{ch}} = c^*_{v,\mathrm{ch}}$, and the GDL drying case has $c_{v,\mathrm{ch}} < c^*_{v,\mathrm{ch}}$.

bound to prevent flooding and maximize membrane water content. A lower bound has yet to be found and is a planned topic of future research. Another implementation issue that needs to be considered is the control of the hydrogen supply. Due to the low-flow rates and low-molecular weight, current sensors may not be able to control hydrogen flow to within the ± 0.05 slm that will likely be required for this application. This issue may also be addressed by the control algorithm, and control of the hydrogen supply is being addressed by industry (e.g. Sugawara, 2003, 2005).

9. Conclusions

It has been established that the liquid water filling dynamics within the GDL of a PEMFC are stable for the semi-analytic model described in McCain et al. (accepted for publication), thus channel water mass stabilization implies fuel cell water stability.

The semi-analytic model has been shown to have ranges of state variables where equilibria do not exist. Further, a general equilibrium condition that can be attained and controlled by manipulation of the channel water vapor concentration has been found and proposed as an efficient control objective due to its minimization of flooding and maximization of water vapor concentration at the membrane. The understanding of instability in the channel and influence of channel conditions on the GDL, stability in the GDL, and the ability to control the BCs using practical inputs and outputs imply that boundary value control for fuel cell water management may be feasible.

Appendix A.

To show stability of the liquid water distribution within the GDL for the BCs described in Section 2.3, we first perform a general linearization of the liquid PDE with the assumption that $s > s_{\text{im}}$ for $0 \leqslant x \leqslant L$, which will result in non-zero liquid mass flow from the GDL to the channel. A simple transformation of the linearized system is then applied to facilitate the subsequent Lyapunov stability analysis. Finally, reference tables for variables, parameters and their values, subscripts and superscripts are included.

A.1. Linearization of the continuous PDE

In preparation for local stability analysis, we start by deriving a general linear PDE for the liquid water anode distribution. Assuming $s > s_{\text{im}}$, linearization of the GDL liquid PDE (38) is accomplished by substitution of a perturbation from an equilibrium distribution $S(x,t) = S_o(x) + \Delta S$,

$$\frac{\partial s}{\partial t} = \frac{b_1}{(b_2+1)} \frac{\partial^2}{\partial x^2}((S_o(x) + \Delta S)^{b_2+1}) + f_o(x), \tag{61}$$

where $f_o(x) = M_v \gamma / \rho_l (\alpha_1 \, e^{\beta x} + \alpha_2 \, e^{-\beta x})$. A linear approximation for polynomial expansion is

$$(S_o(x) + \Delta S)^{b_2+1} \simeq S_o(x)^{b_2+1} + (b_2+1) S_o(x)^{b_2} \Delta S. \tag{62}$$

Inserting Eq. (62) into Eq. (61), it can be seen that the initial steady-state solution is embedded within

$$\frac{\partial s}{\partial t} = \overbrace{\frac{b_1}{(b_2+1)} \frac{\partial^2}{\partial x^2} S_o(x)^{b_2+1} + f_o(x)}^{\dot{s}_o = 0} + b_1 \frac{\partial^2}{\partial x^2}(S_o(x)^{b_2} \Delta S).$$

Since,

$$\Delta S = \frac{\Delta s}{(1 - s_{\text{im}})}, \tag{63}$$

we get

$$\Delta \dot{s} = \frac{b_1}{(1 - s_{\text{im}})} \frac{\partial^2}{\partial x^2}(S_o^{b_2} \Delta s). \tag{64}$$

Defining $w \triangleq S_o^{b_2} \Delta s$ results in,

$$w_t = K_2 S_o^{b_2} w_{xx} = \psi(x) w_{xx}, \tag{65}$$

where $K_2 = b_1/(1 - s_{\text{im}})$ and $\psi(x) \triangleq K_2 S_o^{b_2}$.

The BCs of the new PDE are found by substituting the original BC into the transformation. For the $x = 0$ Neumann BC,

$$w_x(0,t) = b_2 S_o^{b_2 - 1} \frac{\partial S_o}{\partial x} \Delta s + S_o^{b_2} \frac{\partial (\Delta s)}{\partial x} = 0, \tag{66}$$

because both the initial steady-state and perturbation distributions must satisfy the zero-slope requirement at $x = 0$.

For the $x = L$ Dirchlet BC,

$$w(L,t) = S_o^{b_2}(L) \Delta s(L) = 0, \tag{67}$$

because a fixed $x = L$ BC, which is a requirement for steady-state conditions, requires $\Delta s(L)$ remain zero. Thus for any constant BC at $x = L$, the BC of the transformed system will be zero.

A.2. Liquid GDL stability

Modifying the steps described in Krstic et al. (2008) to fit our application, a Lyapunov stability analysis is applied to the plant of the transformed system (65). $L = 1$ is taken for convenience, since a coordinate transformation $z = x/L$ could be implemented without loss of generality.

Using the candidate Lyapunov function,

$$V(w, w_x) = \frac{1}{2} \int_0^1 \frac{w^2(x,t)}{\psi(x)} \, dx + \frac{1}{2} \int_0^1 w_x^2(x,t) \, dx, \tag{68}$$

where it should be noted that $\psi(x) > 0$ over the range $x \in [0,1]$, and thus V is defined over the entire range.

Taking the time derivative of the candidate Lyapunov function,

$$\dot{V} = \int_0^1 \left(\frac{w w_t}{\psi(x)} - \frac{1}{2} \frac{w^2 \psi_t(x)}{\psi(x)^2} \right) dx + \int_0^1 w_x w_{tx} \, dx, \tag{69}$$

where $\psi_t(x) = 0$ since $\psi(x)$ is not a function of time. Substituting the transformed PDE, $w_t = \psi(x) w_{xx}$, and integrating by parts,

$$\dot{V} = \int_0^1 w w_{xx} \, dx + \int_0^1 w_x w_{tx} \, dx, \tag{70}$$

$$\dot{V} = w w_x \Big|_0^1 - \int_0^1 w_x^2 \, dx + w_x w_t \Big|_0^1 - \int_0^1 \psi w_{xx}^2 \, dx. \tag{71}$$

From Eqs. (66) and (67) and $w_t(1) = 0$,

$$\dot{V} = - \int_0^1 w_x^2 \, dx - \int_0^1 \psi w_{xx}^2 \, dx. \tag{72}$$

Since $\dot{V} \leqslant 0$, we have stability in the sense of Lyapunov. To show exponential stability, recognize that $0 < \psi_{\min} \leqslant \psi$, and apply Poincaré's inequality to show

$$- \int_0^1 w_x^2 \, dx \leqslant - \gamma \psi_{\min} \int_0^1 \frac{w^2}{\psi} \, dx \tag{73}$$

and

$$- \int_0^1 \psi w_{xx}^2 \, dx \leqslant - \gamma \psi_{\min} \int_0^1 w_x^2 \, dx, \tag{74}$$

Table 1
Nomenclature and parameter values

Parameter	Value	Meaning
γ	900 (s^{-1})	Evaporation rate
A_{fc}	0.03 (m^2)	FC active area
α_w	11.5	Tuned membrane transport parameter
S_δ	0.0003	Boundary condition at $S(x_{fr}, t)$
s_{im}	0.1	Immobile saturation
R	8.31477 (J/molK)	Universal gas constant
D_{H_2}	1.24e−4 (m^2/s)	Diffusion coeffcients
D_{O_2}	3.45e−5 (m^2/s)	
D_v	3.00e−5 (m^2/s)	
M_{H_2}	0.002 (kg/mol)	H_2 molar mass
M_{O_2}	0.032 (kg/mol)	O_2 molar mass
M_v	0.018 (kg/mol)	Water molar mass
ρl	997 (kg/m^3)	Density
ε	0.5	Porosity
t_{mb}	3.81e−5 (m)	mb Thickness
V_{ch}	2.0e−5 (m^3)	ch Volume
L	5e−4 (m)	GDL thickness
n	3 or 10	Number of sections
dx	L/n (m)	Discretization width
V_p	εA_{fc} dx (m^3)	GDL pore vol.
k	9.344e−7 (m s)	Orifice const.

Table 2
Notation for variables, parameters, subscripts, and superscripts

Super/Subscript	Meaning	Super/Subscript	Meaning
j	Constituent (H_2, O_2, etc.)	mb	Membrane
v, l, w, gas	Vapor, liquid, water, gas		
e	Electrode (an,ca)	ss	Steady-state
R (J/molK)	Universal	GDL	Gas diffusion layer
lin	Linear model	exp	Exponential
rct	Reaction	fr	Mobile front
air	Air	amb	Ambient
in, out	ch in, out	sat	Saturation
Variable	**Meaning**	**Variable**	**Meaning**
$W_{j,e}$ (kg/s)	Mass flow rate	$N_{j,e}$ (mol/m^2s)	Molar flux
α_1	Anode $c_v(x)$	v_1	Cathode $c_v(x)$
α_2	Solution coeffs.	v_2	Solution coeffs.
I_{st} (A)	Stack current	m_o (mol/m^4)	$dc_v/dx|_{s(x,t)=0}$
λ	Water content	$c_j(x)$ (mol/m^3)	Concentration
T_{st} (K)	Stack temp.	$s_e(x,t)$	Saturation
$D_j^{s_{im}}$ (m^2/s)	$D_j(s)$ w/$s = s_{im}$	$S_e(x,t)$	Reduced saturation
P (Pa)	Pressure	m (kg)	Mass
$D_j(s)$ (m^2/s)	Effective diffusivity		

where $\gamma = \frac{1}{4}$. Then,

$$\dot{V} \leqslant -\gamma\psi_{\min}\left(\int_0^1 \frac{w^2}{\psi}\,dx + \int_0^1 w_x^2\,dx\right), \tag{75}$$

which becomes

$$\dot{V} \leqslant -2\gamma\psi_{\min}V \tag{76}$$

indicating that $V \to 0$ exponentially as $t \to \infty$. To show pointwise convergence, use Agmon's inequality (with $w(1,t) = 0$),

$$\max_{x\in[0,1]} |w(x,t)|^2 \leqslant 2\|w(\cdot,t)\| \cdot \|w_x(\cdot,t)\|, \tag{77}$$

and the inequality $2\|a\| \cdot \|b\| \leqslant \|a\|^2 + \|b\|^2$ to find,

$$\max_{x\in[0,1]} |w(x,t)|^2 \leqslant \|w(\cdot,t)\|^2 + \|w_x(\cdot,t)\|^2, \tag{78}$$

where $\|\cdot\|$ denotes the L2-norm. Since $\psi(x) > 0$ for all x and $V \to 0$, $\|w(x,t)\| \to 0$ and $\|w_x(x,t)\| \to 0$ as $t \to \infty$, implying,

$$\max_{x\in[0,1]} |w(x,t)| \to 0 \quad \text{as } t \to \infty. \tag{79}$$

Pointwise convergence is thus shown, and the liquid water distribution within the GDL is exponentially stable.

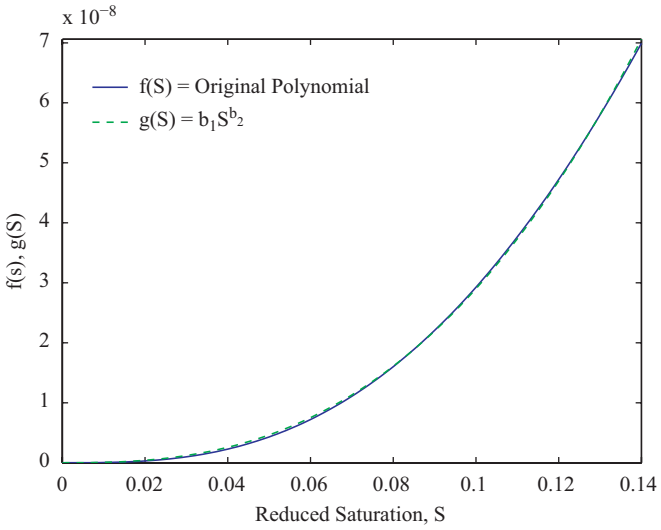

Fig. 8. Demonstration of the accuracy of the single term polynomial fit in S to the original multi-term polynomial from the Leverett function-based capillary pressure empirical expression.

A.3. Nomenclature

A description of the parameter, variables, subscripts, and superscripts can be found in Tables 1 and 2.

A.4. Single term fit

A graph demonstrating the accuracy of the single term polynomial fit,

$$\frac{K}{\mu}S^3\frac{\delta p_c}{\delta S} \approx b_1 S^{b_2}, \tag{80}$$

taken over a range of S roughly twice as large as typically seen in simulation, is shown in Fig. 8.

References

Baschuk, J., Li, X., 2000. Modelling of polymer electrolyte membrane fuel cells with variable degrees of water flooding. Journal of Power Sources 86, 181–196.

Djilali, N., Lu, D., 2002. Influence of heat transfer on gas and water transport in fuel cells. International Journal of Thermal Science 41, 29–40.

Gan, M., Chen, L.D., 2006. Analytic solution for two-phase flow in PEMFC gas diffusion layer. In: ASME Fuel Cell 2006, ASMEFC2006-97104, Irvine, CA, USA.

Grötsch, M., Mangold, M., 2007. A two-phase PEMFC model for process control purposes. Chemical Engineering Science 63, 434–447.

Karnik, A.Y., Sun, J., 2005. Modeling and control of PEMFC system with an anode recirculation. In: 2005 Third International Conference on Fuel Cell Science, Engineering and Technology, Ypsilanti, MI.

Krstic, M., et al., 2008. Boundary control of PDEs: A Course on Backstepping Designs. SIAM.

Lauzze, C., Chmielewski, D.J., 2006. Power control of a polymer electrolyte membrane fuel cell. Journal of Industrial Engineering Chemical Research 45, 4661–4670.

Mahadevan, J., Sharma, M., Yortsos, Y., 2006. Flow-through drying of porous media. American Institute of Chemical Engineers Journal 52 (7), 2367–2380.

Mazumder, S., Cole, J.V., 2003. Rigorous 3d mathematical modeling of PEM fuel cells: 2 model predictions with liquid transport. Journal of the Electrochemical Society 150 (11), A1510–A1517.

McCain, B.A., Stefanopoulou, A.G., Kolmanovsky, I.V., 2007. A multi-component spatially-distributed model of two-phase flow for estimation and control of fuel cell water dynamics. In: 46th IEEE Conference on Decision and Control, CDC2007-1455, New Orleans, LA, USA.

McCain, B.A., Stefanopoulou, A.G., Kolmanovsky, I.V., A dynamic semi-analytic channel-to-channel model of two-phase water distribution for estimation and control of fuel cells. IEEE Transactions in Control Systems Technology, accepted for publication.

McKay, D.A., Siegel, J.B., Ott, W.T., Stefanopoulou, A.G., 2008. Parameterization and prediction of temporal fuel cell voltage behavior during flooding and drying conditions. Journal of Power Sources 178 (1), 207–222.

Meng, H., Wang, C.Y., 2004. Electron transport in PEFCs. Journal of the Electrochemical Society 151 (3), A358–A367.
Mufford, W.E., Strasky, D.G., 2006. Power control system for a fuel cell powered vehicle. US patent 5 771 476.
Nam, J.H., Kaviany, M., 2003. Effective diffusivity and water-saturation distribution in single- and two-layer PEMFC diffusion medium. International Journal of Heat and Mass Transfer 46, 4595–4611.
Natarajan, D., Nguyen, T.V., 2001. A two-dimensional, two-phase, multicomponent, transient model for the cathode of a proton exchange membrane fuel cell using conventional gas distributors. Journal of the Electrochemical Society 148 (12), A1324–A1335.
Owejan, J.P., Owejan, J.E., Tighe, T.W., Gu, W., Mathias, M., 2007. Investigation of fundamental transport mechanism of product water from cathode catalyst layer in PEMFCs. In: 5th Joint ASME/JSME Fluids Engineering Conference, San Diego, CA, USA.
Promislow, K., Stockie, J., 2001. Adiabatic relaxation of convective-diffusive gas transport in a porous fuel cell electrode. SIAM Journal of the Applied Mathematics 62, 180–205.
Promislow, K., Chang, P., Haas, H., Wetton, B., 2008. Two-phase unit cell model for slow transients in polymer electrolyte membrane fuel cells. Journal of the Electrochemical Society 155, A494.
Pukrushpan, J.T., Stefanopoulou, A.G., Peng, H., 2000. Control of Fuel Cell Power Systems: Principles, Modeling, Analysis and Feedback Design. Springer, New York.
Shah, A.A., Kim, G.S., Gervais, W., Young, A., Promislow, K., Harvey, D., 2006. The effects of water and microstructure on the performance of polymer electrolyte fuel cells. Journal of Power Sources 160, 1251–1268.
Siegel, J.B., Stefanopoulou, A.G., 2008. Modeling and visualization of fuel cell water dynamics using neutron imaging. In: 2008 American Control Conference, Seattle, WA.
Siegel, N.P., Ellis, M.W., Nelson, D.J., von Spakovsky, M.R., 2006. A two-dimensional computational model of a PEMFC with liquid water transport. Journal of Power Sources 128 (1), 173–184.
Smyshlyaev, A., Krstic, M., 2005. On control design for PDEs with space-dependent diffusivity or time-dependent reactivity. Automatica 41, 1601–1608.
Springer, T.E., Zawodzinski, T.A., Gottesfeld, S., 1991. Polymer electrolyte fuel cell model. Journal of the Electrochemical Society 138 (8), 2334–2342.
Sugawara, T., 2003. Fuel cell power generation system. US patent 6617066.
Sugawara, T., 2005. Variable flow-rate ejector and a fuel cell having the same. US patent 6858340.
Suh, K.W., Stefanopoulou, A.G., 2007. Control and coordination of air compressor and voltage converter in load-following fuel cells. International Journal of Energy Research 29, 1167–1189.
Sun, J., Kolmanovsky, I.V., 2004. Robust reference governor for fuel cell starvation protection. IEEE Transactions in Control Systems Technology 13 (6), 911–920.
Vynnycky, M., 2007. On the modelling of two-phase flow in the cathode gas diffusion layer of a polymer electrolyte fuel cell. Applied Mathematics and Compution 189, 1560–1575.
Zenith, F., Skogestad, S., 2007. Control of fuel cell power output. Journal of Process Control 17, 333–347.
Zhang, F.Y., Yang, X.G., Wang, C.Y., 2006. Liquid water removal from a polymer electrolyte fuel cell. Journal of the Electrochemical Society 153 (2), A225–A232.